ACS Biomaterials SCIENCE & ENGINEERING

pubs.acs.org/journal/abseba

Article

Measuring the Effects of Cytokines on the Modification of Pericellular Rheology by Human Mesenchymal Stem Cells

Maryam Daviran,[§] John A. McGlynn,[§] Jenna A. Catalano, Hannah E. Knudsen, Kilian J. Druggan, Kiera J. Croland, Amanda Stratton, and Kelly M. Schultz*

Cite This: https://doi.org/10.1021/acsbiomaterials.1c00871

Read Online

ACCESS | Metrics & More | Article Recommendations | Supporting Information

ABSTRACT: Implantable hydrogels are designed to treat wounds by providing structure and delivering additional cells to damaged tissue. These materials must consider how aspects of the native wound, including environmental chemical cues, affect and instruct delivered cells. One cell type researchers are interested in delivering are human mesenchymal stem cells (hMSCs) due to their importance in healing. Wound healing involves recruiting and coordinating a variety of cells to resolve a wound. hMSCs coordinate the cellular response and are signaled to the wound by cytokines, including transforming growth factor-β (TGF-β) and tumor necrosis factor-α (TNF-α), present *in vivo*. These cytokines change hMSC secretions, regulating material remodeling. TGF-β, present from inflammation through remodeling, directs hMSCs to reorganize collagen, increasing extracellular matrix (ECM) structure. TNF-α, present primarily during inflammation, cues hMSCs to clear debris and degrade ECM. Because cytokines change how hMSCs degrade their microenvironment and are naturally present in the wound, they also affect how hMSCs migrate out of the scaffold to conduct healing. Therefore, the effects of cytokines on hMSC remodeling are important when designing materials for cell delivery. In this work, we encapsulate hMSCs in a polymer−peptide hydrogel and incubate the scaffolds in media with TGF-β or TNF-α at concentrations similar to those in wounds. Multiple particle tracking microrheology (MPT) measures hMSC-mediated scaffold degradation in response to these cytokines, which mimics aspects of the *in vivo* microenvironment post-implantation. MPT uses video microscopy to measure Brownian motion of particles in a material, quantifying structure and rheology. Using MPT, we measure increased hMSC-mediated remodeling when cells are exposed to TNF-α and decreased remodeling after exposure to TGF-β when compared to untreated hMSCs. This agrees with previous studies that measure: (1) TNF-α encourages matrix reorganization and (2) TGF-β signals the formation of new matrix. These results enable material design that anticipates changes in remodeling after implantation, improving control over hMSC delivery and healing.

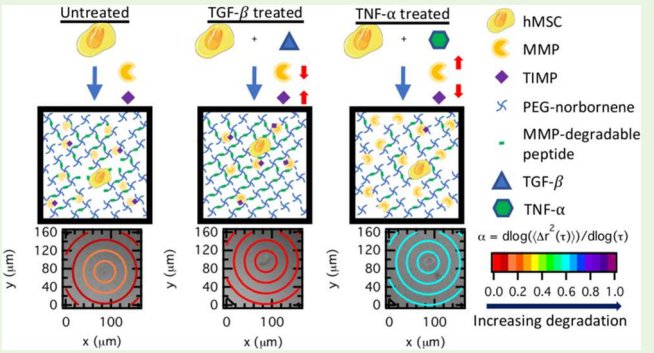

KEYWORDS: *hydrogels, human mesenchymal stem cells, cytokines, multiple particle tracking microrheology*

INTRODUCTION

Hydrogels are an important class of materials for the treatment of wounds.[1−12] These materials are designed to be implanted into the wounded area to provide structure to the wound, allowing it to heal more effectively. In addition to providing structure, hydrogels can also serve as vehicles to deliver additional cells to aide, progress, or enhance the healing process.[6,7,13] A common cell type targeted for delivery is the human mesenchymal stem cell (hMSC). hMSCs are chosen for cell delivery due to their importance in wound healing, including modulating the immune response and controlling the formation of new tissue.[14−20] To design a scaffold that can effectively deliver hMSCs, the material must be able to be remodeled by encapsulated cells and also cue cells to undergo basic cellular functions, a critical feedback loop. hMSCs remodel their surroundings irreversibly using cell-secreted enzymes called matrix metalloproteinases (MMPs) and reversibly by applying forces on the network using cytoskeletal tension. hMSCs also regulate matrix degradation by secreting tissue inhibitor of metalloproteinases (TIMPs), which bind to MMPs on secretion, preventing their activity immediately around the cell. MMP−TIMP complexes unbind further away from the cell, resulting in spatial differences in MMP activity and rheology.[3,9] Within a hydrogel, cell function can be manipulated through the addition of physical cues, such as

Received: July 1, 2021
Accepted: October 28, 2021

matrix stiffness, and chemical cues, such as the addition of a protein like bone morphogenetic protein-2 to induce osteogenesis.[8,21] Scaffolds designed to enable cell-mediated remodeling allow hMSCs to migrate out of the delivery material and into the native wound environment to orchestrate the healing process.[4,8,11,22−24]

After implantation, hMSCs are not only influenced by cues within the hydrogel scaffold, they also receive cues from the native wound environment. The wound environment includes several chemicals, including cytokines, which manipulate the response of all cells required to heal the wound. Two cytokines present in the wound as part of the wound healing cascade, transforming growth factor-β (TGF-β) and tumor necrosis factor-α (TNF-α), affect hMSC secretions of MMPs and TIMPs, resulting in changes in cell-mediated scaffold degradation.[14,25−30] This change in cell-mediated scaffold degradation will affect cell function within the hydrogel scaffold and change the feedback between the material rheology presented to the encapsulated cell and the cell-engineered rheology. This feedback is important because the rheology of the local cell microenvironment has been shown to manipulate cell functions including cell speed, morphology, and lineage specification.[1−4,8,9,11,31] Therefore, when designing materials for *in vivo* cell delivery, these changes must be accounted for. In this work, we characterize the effect of TGF-β and TNF-α on hMSC remodeling to enable more effective materials to be designed for hMSC delivery. Here, we add another aspect of the wound environment, providing a more accurate representation of how these materials will perform when implanted *in vivo* where cytokines are present.

hMSCs migrate *in vivo* out of the bone marrow niche to the wound site in response to a gradient of signaling molecules from a wound.[14,19] These signaling molecules are released during the first stage of the wound healing process, hemostasis.[14] After reaching the wound, hMSCs are directly involved in the next three stages of wound healing: inflammation, proliferation, and remodeling. Their activity is, in part, controlled by cytokines present at the wound site. In the inflammation stage, they regulate the degradation of damaged extracellular matrix (ECM) by increasing MMP secretions.[14,28] During proliferation, they produce growth factors and recruit other reparatory cells. Finally, in the remodeling phase, they regulate the development of new matrix by controlling MMP secretions and the deposition of collagen.[14] Because of the significant role hMSCs have in wound healing, delivering supplemental hMSCs to a wound has been studied as a treatment for chronic wounds, wounds that remain in an inflamed state, and enhanced wound repair.[7,13,20] Much of the previous work on scaffold design for hMSC delivery has focused on hMSC interactions with material when exposed to cell growth media. Exploring changes when a cell-laden scaffold is exposed to signaling molecules present in the wound environment, such as TNF-α and TGF-β, requires further study.

TNF-α is present primarily in the inflammatory stage.[14,26] It is produced by macrophages present at the wound site as they clear debris and bacteria. It suppresses the production of ECM proteins and increases the secretion of MMPs in chorionic cells, endometrial stromal cells, macrophages, and hMSCs.[25,28−30,32] It also inhibits the production of TIMPs, facilitating network degradation by secreted MMPs.[25] TNF-α is also present in chronic wounds.[25,33] While TNF-α increases degradation of the matrix and prevents new ECM formation, TGF-β exposure results in increased TIMP secretion, inhibiting MMPs, and upregulates the formation of fibronectin, contributing to the formation of new matrix in the proliferative and remodeling phases.[27,34,35] Tethering TGF-β to a network has also been found to induce chondrogenesis in encapsulated hMSCs.[36] TGF-β is not found in chronic wounds, suggesting that its absence contributes to chronic wound formation.[33] Understanding how each of these cytokines affects hMSC function is important in the use of hMSCs as a wound repair tool because these cytokines will be present *in vivo* when hMSCs are delivered from an implantable scaffold.

Synthetic implantable materials are designed to improve wound healing outcomes by delivering additional hMSCs to the wounded area and providing structure to the wound.[1−5,7−9,13,37,38] These scaffolds can incorporate physical and chemical cues which direct hMSC function, such as a physical gradient in stiffness inducing durotaxis or a chemokine gradient inducing chemotaxis.[21,39−42] Our scaffold uses a four-arm poly(ethylene glycol)-norbornene (PEG-norbornene) molecule as its backbone, which is cross-linked with an MMP-degradable peptide sequence to form a gel network.[1−4,7−11,13] The inclusion of this peptide allows the material to be degraded by cell-secreted MMPs.[2] We also include an adhesion ligand, CRGDS, enabling cells to attach to the network using integrins and pull on the scaffold using cytoskeletal tension.[5,8,11] This platform has been extensively studied and results in high cell viability after three-dimensional (3D) encapsulation.[3−5,9] Our scaffold mimics aspects of the native microenvironment, allowing us to systematically add complexity. While considerable work has been done to understand how hMSCs interact with a variety of materials, more could be done to better understand how cytokines present in the pericellular region affect cell-mediated remodeling of their microenvironment. To study how hMSCs exposed to TGF-β or TNF-α remodel their local microenvironment, we use multiple particle tracking microrheology (MPT), a technique that measures spatiotemporal rheology around an individual hMSC migrating in our hydrogel.[1−4,8,9,11,43]

Multiple particle tracking microrheology is a passive microrheological technique that is used to characterize the material around migrating hMSCs in our hydrogel.[1,3,4,8,9,11,43] MPT uses video microscopy to measure the Brownian motion of embedded probe particles in the material to characterize rheology.[44−50] Spatial changes in rheology are determined by splitting the viewing area into different regions and measuring the motion of the particles in each region separately.[1,3,8,9,11] Because TGF-β and TNF-α change hMSC remodeling strategies, measurements of pericellular rheology are different when these cytokines are present.[1,3,4,8,9,11] Additionally, these changes in pericellular rheology significantly impact cell motility, which will change how effective a material is at hMSC delivery. This makes MPT especially useful for understanding how individual hMSCs remodel their local microenvironment differently in the presence of cytokines.

In this work, we characterize the changes in pericellular rheology around migrating hMSCs exposed to TGF-β or TNF-α in the fluid environment. We compare the remodeling around these cells to pericellular remodeling around untreated hMSCs. We measure increased remodeling around hMSCs treated with TNF-α and decreased or similar remodeling around hMSCs treated with TGF-β relative to untreated hMSCs. We hypothesize that TNF-α increases hMSC

https://doi.org/10.1021/acsbiomaterials.1c00871
ACS Biomater. Sci. Eng. XXXX, XXX, XXX−XXX

remodeling because it increases the secretion of MMPs and decreases secretion of TIMPs. TGF-β decreases remodeling because previous work has shown that it decreases the hMSC secretion of MMPs and increases the secretion of TIMPs. These changes in cell secretions directly affect how the pericellular region evolves over time. We measure that average cell speeds are similar regardless of the cues presented in the fluid environment. Finally, we measure that cells that have remodeled their microenvironments more are more persistent, migrating consistently in the same direction as opposed to a random migration pattern. Specifically, hMSCs which have remodeled the pericellular region past the gel−sol transition are highly persistent. This is measured for hMSCs treated with both cytokines, and the largest effect is measured in TNF-α treated hMSCs. We hypothesize that these results are due to changes in cell behavior after exposure to these cytokines. These results provide important information about how hMSCs will degrade their surroundings when implanted in the native wound environment, which is important for their use as a cell delivery vehicle.

EXPERIMENTAL SECTION

hMSC Culture. hMSCs are obtained from Lonza in passage 2 and plated in 150 cm^2 tissue culture Petri dishes (Corning) with growth media. Growth media consists of 50 U mL^{-1} penicillin/streptomycin (Life Technologies), 1 ng mL^{-1} recombinant human fibroblast growth factor (hFGF, PeproTech), 0.5 μg mL^{-1} Fungizone (Life Technologies), and 10% fetal bovine serum (FBS, Life Technologies) in a low-glucose Dulbecco's modified Eagle's medium (DMEM, Life Technologies). Cells are passaged at 90% confluency. In all experiments, hMSCs are used in passages 2−6.

Hydrogel Scaffold. Our hydrogel scaffold is composed of four-arm star poly(ethylene glycol) (PEG)-norbornene (3 mM, M_n = 20 000 g mol^{-1}, f = 4, where f is the number of functional groups, Sigma-Aldrich and JenKem Technology) cross-linked with an MMP-degradable peptide sequence, KCGPQG↓IWGQCK (3.9 mM, M_n = 1305 g mol^{-1}, f = 2, ↓ is the cleavage site, Bachem). This peptide sequence is readily cleaved by hMSC-secreted MMPs.[2,51,52] Once the cross-linker has been broken by cell-secreted enzymes, it cannot reform. This results in permanent degradation of the scaffold by hMSCs. This enables cells to degrade their surrounding microenvironment, spread and migrate within the scaffold.[4,5,37,52] In the absence of cells, α is uniform throughout the hydrogel and does not change with time, and no degradation is measured.[3]

In all experiments, hydrogels are formed with a thiol:ene stoichiometric ratio of 0.65. This low thiol:ene ratio results in a hydrogel with a stiffness similar to adipose tissue when swollen ($G' \approx$ 300 Pa). This scaffold is widely used for cell encapsulation and results in high cell viability.[5,52,53] An adhesion ligand, CRGDS (1 mM, M_n = 594 g mol^{-1}, f = 1, American Peptide Inc.), is tethered to the scaffold to facilitate cell attachment to the network. To initiate gelation, lithium phenyl-2,4,6-trimethylbenzoylphosphinate (LAP, 1.7 mM), a highly water-soluble photoinitiator, is added to the precursor solution.[54] 0.2% solids/volume of fluorescently labeled carboxylated polystyrene probe particles ($2a$ = 0.97 ± 0.01 μm, a is the probe particle radius, Polysciences, Inc.) are added to the precursor solution to enable MPT measurements. The pH of the precursor solution is adjusted to 7 by adding 15 mM sodium hydroxide (Fisher Scientific) to the solution as needed. Finally, hMSCs are suspended in 1× phosphate buffered saline (1× PBS, Life Technologies) and added to the precursor solution at a final concentration of 2×10^5 cells mL^{-1}. This hydrogel composition is commonly used and well characterized from previous work.[2,4,5,53,55]

The precursor solution is mixed and pipetted into a sample chamber, described below. The sample chamber is placed under UV light at 5 mW cm^{-2} (365 nm light, UVP, LLC) for 3 min. The polymers in the precursor solution react by step-growth photopolymerization, resulting in hMSCs evenly distributed within the 3D gel network. Immediately after gelation, sample chambers are filled with 4 mL of growth media without hFGF and incubated at 37 °C and 5% CO_2.

To characterize how hMSCs respond to each cytokine, 100 ng mL^{-1} of TGF-β1 (referred to as TGF-β, PeproTech) or TNF-α (PeproTech) are added to cell media immediately after 3D cell encapsulation and incubated overnight at 37 °C and 5% CO_2. This cytokine concentration is chosen to mimic the concentration in a wounded area of the body.[56]

Data are taken 2−4 days after cell encapsulation. Data are collected at these times because this gives enough time for cells to spread, adjust to their environment, and resume normal function.

Device Fabrication. Cell-laden hydrogels are made in glass-bottomed Petri dishes (d = 35 mm, no. 1.5 glass coverslip, MatTek Corporation). The design of these sample chambers has been detailed elsewhere.[2,3,8,9,11,43] Briefly, a cylindrical polydimethylsiloxane (PDMS, Dow Corning) tube is made from a flat PDMS sheet using 6 and 10 mm disposable biopsy punches (Acuderm Inc.). The tube is ≈6 mm tall and has an outer diameter of 10 mm and an inner diameter of 6 mm. To make PDMS sheets, a silicone elastomer base is mixed with a curing agent at a ratio of 10:1 (ratio recommended by manufacturer, Dow Corning). The solution is degassed and cured overnight at 65 °C. PDMS tubes are cut out using biopsy punches and attached to the glass bottom of the Petri dishes using uncured PDMS and cured at 65 °C overnight. This PDMS tube is used to hold the hydrogel precursor solution before gelation and limits particle drift in the sample as the hydrogel scaffold is degraded by cell-secreted enzymes.

Sample chambers are sterilized with 70% ethanol prior to the addition of the hydrogel precursor solution. After sterilization, 17 μL of the precursor solution is pipetted into the PDMS tubes and photopolymerized as described above. This volume of precursor solution is chosen so that the hydrogel swells isotropically within the sample chamber and is not inhibited by the chamber walls.

Multiple Particle Tracking Microrheology. hMSC-mediated degradation and remodeling of the pericellular region is characterized using multiple particle tracking microrheology (MPT). MPT measures the Brownian motion of probe particles embedded in the material using video microscopy.[43,44,46,50,57,58] Fluorescently labeled carboxylated polystyrene probe particles ($2a$ = 0.97 ± 0.01 μm, Polysciences, Inc.) are added to the precursor solution prior to gelation. Particle concentration, size, and surface chemistry are chosen to limit particle−particle, particle−polymer, and particle−cell interactions.[43,46,48,57]

MPT data are collected using an inverted microscope (Zeiss Observer Z1, Carl Zeiss AG) with a 63× water immersion objective (N.A. 1.3, 1× optovar, Carl Zeiss AG). A high-speed camera (1024 × 1024 pixels, Miro M120, Vision Research Inc.) is used to record the Brownian motion of probe particles with a frame rate of 30 frame s^{-1} for a total of 800 frames with an exposure time of 1000 μs.[45,50,57] These parameters are chosen to minimize static and dynamic particle tracking errors.[58] To ensure cell survival, the microscope is fit with an incubation chamber to keep the temperature at 37 °C and provide 5% CO_2 during data acquisition.

To collect data, first a cell is located within the hydrogel and positioned roughly in the center of the field of view. This allows the cell to move approximately 80 μm in the x−y plane without leaving the frame. After locating the cell, a brightfield image is taken to record its location. Immediately after taking the brightfield image, a video of particle motion is taken using fluorescence microscopy. This procedure is repeated every 4−6 min for up to an hour unless the cell leaves the field of view or goes out of focus. The stage position is not changed until a new cell is located and the process begins again.

Classical tracking algorithms are used to identify the brightness-weighted centroid of each particle within each frame of the collected videos.[57,59] Particle positions in each frame are linked into a trajectory, using a probability distribution function (PDF) that accounts for the Brownian motion of a single particle.[57,59] The ensemble-averaged mean-squared displacement (MSD), $\langle \Delta r^2(\tau) \rangle$, is

https://doi.org/10.1021/acsbiomaterials.1c00871
ACS Biomater. Sci. Eng. XXXX, XXX, XXX−XXX

calculated from these trajectories using $\langle \Delta r^2(\tau) \rangle = \langle \Delta x^2(\tau) \rangle + \langle \Delta y^2(\tau) \rangle$, where τ is the lag time or separation time between frames and x and y are coordinate directions in 2D.[43,44,48,59,60] Brownian motion of probe particles is related to material and rheological properties. For example, the MSD is directly related to the creep compliance, $J(\tau)$, using the generalized Stokes−Einstein relation

$$\langle \Delta r^2(\tau) \rangle = \frac{k_B T}{\pi a} J(\tau) \tag{1}$$

where $k_B T$ is the thermal energy and a is the probe particle radius.

The logarithmic slope of the MSD, α, is a variable used to quantify the state of the material, where

$$\alpha = \left. \frac{d \log \langle \Delta r^2(\tau) \rangle}{d \log \tau} \right|_{0.033 \le \tau \le 1s} \tag{2}$$

α is a measure of the mobility of the particles, which is used to determine the state of the material they are embedded in. $\alpha \to 0$ indicates that probe particles are immobilized within a gel scaffold. $\alpha = 1$ indicates that particles are freely diffusing in a liquid. α values between 0 and 1 indicate that the material is a viscoelastic gel or liquid.[61−65] The transition of the material from a gel to a liquid is determined by calculating the critical relaxation exponent, n, which will be discussed further in the Results and Discussion section. Microrheological measurements are analyzed at the shortest lag times (0.033−1 s). At these short lag times, the longest relaxation time of the material is measured. Since the shortest lag times are used, these measurements also have a large number of points, resulting in accurate measurements.

While the sample chamber used for these measurements is designed to prevent drift, some drift can inevitably occur especially in samples that are highly degraded. Sample drift can also be caused by the cell moving in the material and applying forces to the network and is not solely the result of the entire sample translating. For this reason, we measure a region in the vicinity but without a cell and determine if drift is occurring in the same direction. If there is drift in the region without cells, the drift is corrected; otherwise, it is not corrected.

Cell Speed and Persistence. Cell position is determined using brightfield microscopy. Brightfield images are taken immediately before collecting MPT data for each cell at each time point. After locating the cell ($t = 0$ min), data are collected every 4−6 min around each cell for approximately 20−65 min. The cell center is determined using a program written in MatLab (Mathworks), which incorporates ImageJ (NIH). The outer edge of the cell is traced, and the average location of the points on this trace is the cell center (x_i, y_i). This is analogous to estimating the center of mass of the cell. These cell centers are then used to calculate cell speed, v, during migration. Cell speed between two subsequent measurements, v_{step} (μm h^{-1}), is calculated using

$$v_{step} = \frac{\sqrt{(x_{i+1} - x_i)^2 + (y_{i+1} - y_i)^2}}{t_{i+1} - t_i} \tag{3}$$

where (x_i, y_i) is the initial location of the cell center at t_i and (x_{i+1}, y_{i+1}) is the location of the cell center at the next measurement, t_{i+1}. Average cell speed is then calculated as the average of all v_{step}, which occur during the measurement of that cell.

We also measure cell persistence, which is the tendency of a cell to migrate in the same direction. To measure cell persistence, the cosine of the angle between cell displacements, $\cos\theta$, is measured. $\cos\theta$ is calculated from the dot product of two consecutive cell displacements with vectors $\vec{x}_i$ and $\vec{x}_{i+1}$ using

$$\vec{x}_i \cdot \vec{x}_{i+1} = |\vec{x}_i||\vec{x}_{i+1}| \cos\theta \tag{4}$$

where $|\vec{x}|$ represents the magnitude of vector $\vec{x}$. We use $\cos\theta \gtrsim 0.8$ as a guide to establish cells are moving persistently. This occurs when each subsequent displacement is within at most 37° of the previous displacement.

Data Analysis and Statistics. For each treatment condition (growth media (untreated), TGF-β, and TNF-α incubated cells) at least three biological replicates are measured. For each biological replicate, two gels are made per stock solution. Data are taken 2−4 days after hMSC encapsulation. This time is selected so that we can characterize pericellular regions around cells at all stages of degradation, from shortly after encapsulation to when previous literature by Mazzeo et al. reported the bulk hydrogel degrades.[2] Data are taken on cells throughout the day, and each pericellular region may have a different extent of degradation based on the activity of that individual cell. For this reason, we show data for all cells as an average with a standard deviation to show the spread in the data.

For untreated hMSCs in growth media, 33 cells are characterized on day 2, 28 cells are characterized on day 3, and 33 cells on day 4 post-encapsulation. For hMSCs treated with TGF-β, 30 cells are characterized on day 2, 30 on day 3, and 33 on day 4 post-encapsulation. For hMSCs treated with TNF-α, 33 cells are characterized on day 2, 31 on day 3, and 31 on day 4 post-encapsulation.

To show data of changes in rheological properties with time, data from a single pericellular region is provided in the main text. Representative data is selected by plotting the data for each cell and selecting one which is representative of the data set. Additional data sets are also provided in the Supporting Information (Figures S1−S6).

Statistical significance is determined using the two-sample Kolmogorov−Smirnov test. This test was chosen because it does not rely on an underlying distribution and can measure changes in distribution shape. Two samples are considered statistically significant if $p < 0.05$. Probability density functions are estimated from data using a kernel smoothing function.

RESULTS AND DISCUSSION

This work uses MPT to quantify spatiotemporal pericellular rheology around encapsulated hMSCs when exposed to TGF-β or TNF-α in the fluid environment. We compare these results to cell-mediated re-engineering of the rheology of pericellular regions around untreated hMSCs. First, we quantify pericellular rheology using MPT in each treatment group and relate the extent of remodeling with the change in cellular secretions based on the cytokine present. We then quantify cell speed for each treatment group. Finally, we quantify cellular persistence, the tendency for a cell to migrate in the same direction, and relate it to the degree of remodeling. This shows that hMSCs that have remodeled the scaffold past the gel−sol transition have more persistent migration. MPT and cell speed results show that cytokines signal cells to modify material rheology, which then results in differences in cell motility but does not have a direct impact on cell speed.

MPT measures the Brownian motion of embedded probe particles in the pericellular region.[43,44,48,59,60] The logarithmic slope of the MSD, α, quantifies the viscoelastic state of the material when compared with the critical relaxation exponent, n.[43,44,61,64,66,67] n is the α value that defines the point where the material transitions from a viscoelastic gel, with a sample-spanning polymer network, to a viscoelastic sol, where the sample is a series of disconnected polymer clusters or single polymer chains.[43,44,61,64,66,67] $\alpha < n$ indicates that the material is a gel, while $\alpha > n$ indicates that the material is a sol.[1,4,8,11,43] When α is within the error of the determined n value, the material is in a transitional region, where the material is undergoing a gel−sol phase transition. n has been determined for this material in previous work and is $n = 0.25 \pm 0.05$.[1,3,9,53] n is a material property and does not change with the concentration of cross-links.[1,3,8,9,53] Using n to define the transition between gel and sol, we can quantify cell-mediated

https://doi.org/10.1021/acsbiomaterials.1c00871
ACS Biomater. Sci. Eng. XXXX, XXX, XXX−XXX

rheological changes in the pericellular region for each treatment group.

We begin by measuring temporal pericellular rheology changes around a single cell. Figure 1 shows representative

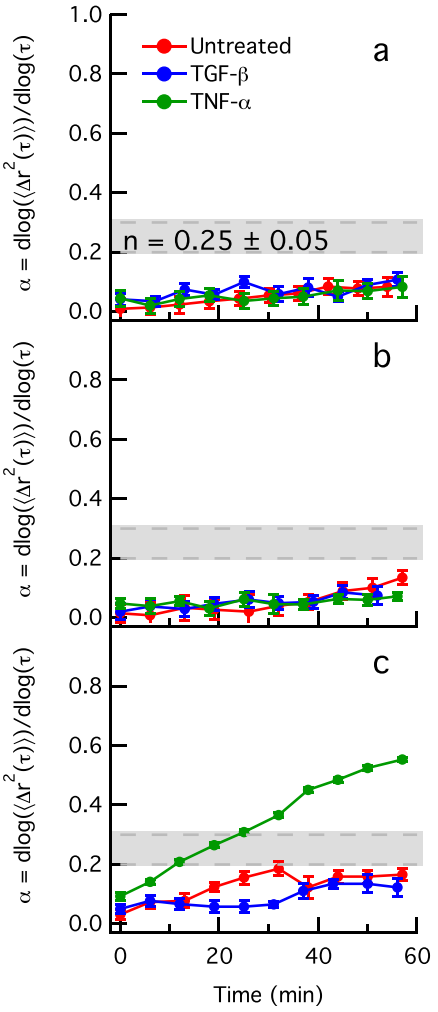

Figure 1. α value measured for the entire pericellular region around untreated, TGF-β or TNF-α treated hMSCs on days (a) 2, (b) 3, and (c) 4 post-encapsulation. The shaded region is the phase-transition region, defined as $n = 0.25 \pm 0.05$, where the material transitions from gel to sol. Each line is data in a single pericellular region, which is representative data for the entire data set. Error bars represent standard error in α.

data of pericellular remodeling around three hMSCs on days 2−4 post-encapsulation (an additional set of data is provided in the Supporting Information in Figure S1). The time the cell is located at the beginning of MPT data acquisition is defined as $t = 0$ min. On day 2 (Figure 1a), little remodeling is measured for all three treatment groups. No cells have remodeled the material to the transition region, and the pericellular region remains a gel. At this early stage of remodeling, hMSCs have only begun to secrete MMPs and have had little time to degrade surrounding material. This is measured by relatively low α values. Additionally, MPT measures similar remodeling for each treatment group. While previous reports have shown that the presence of cytokines affects hMSC secretions,[25,27,29,30,34,35] this change is not great enough to have a significant impact on cell-mediated degradation and changes in pericellular rheology this soon after encapsulation. Day 3 post-encapsulation (Figure 1b) measurements are similar to day 2. Cells have not remodeled enough of the material to transition the scaffold from a gel to a sol.

On day 4 post-encapsulation (Figure 1c), differences in the rheology of the pericellular region become more apparent for hMSCs in each treatment group. α values for all treatments increase with time, measuring that cross-links are being broken by cell-secreted MMPs. The material around the untreated cell does not cross into the transition region during MPT data acquisition (60 min). This indicates that the material surrounding the hMSC remains a gel, but the number of cross-links has decreased. This agrees with previous studies, which have measured that hMSCs have not significantly remodeled their microenvironment.[1,3,4,8,9] The α value for the cell treated with TGF-β is similar to α values for the untreated cell. The small difference that occurs between 20 and 35 min may be due to increased cell motion or a difference in reversible cell-mediated scaffold remodeling or irreversible cell-mediated scaffold degradation. Both remain below the transition region throughout the measurement time. Based on previous reports, we hypothesize that this is because TGF-β increases the production of TIMPs and decreases the production of intracellular proteases including MMPs.[14,68] Both of these factors result in reduced matrix remodeling, which is measured by lower α values around the TGF-β treated cell when compared with α around the untreated cell. In contrast, the cell treated with TNF-α remodels its surrounding material with α values increasing through and above the transition region over the course of the measurement time. α increases past the transition region, indicating that the material has transitioned to a sol and a sample-spanning network is no longer present. While a sample-spanning network is no longer present, there is still a dense concentration of polymer clusters present in the pericellular region for $\alpha > n$. We hypothesize that increased remodeling by the TNF-α treated cell is due to the effects the cytokine has on hMSC secretions. Previous work shows that TNF-α increases the secretion of MMPs and decreases the secretion of TIMPs. This would result in an increase in active MMPs in the pericellular region that break cross-links.[25,29,30] The increase in enzyme and reduction of inhibitor would result in more pericellular remodeling by the hMSC.

Overall, the results in Figure 1 show that for all treatment groups, degradation increases over time due to the cumulative effect of MMPs secreted by the cell degrading the network. Additionally, the effects of the cytokine, TGF-β or TNF-α, on hMSC secretions change the degree hMSCs remodel the pericellular region. The data in Figure 1 is limited, however, because it averages rheological properties over the entire field of view. Previous work has shown that α varies significantly as a function of distance from the cell center.[2−4,8,9,11] Additionally, the difference in spatial pericellular remodeling has been attributed to cytoskeletal tension and the presence of MMPs and TIMPs; the secretion of both molecules has been shown in previous literature to change when TNF-α or TGF-β is in the fluid environment.[2−4,8,9,11,14,25,29,30,68] For these reasons, we analyze changes in pericellular rheology as a function of distance from the cell center for all treatment groups.

To measure spatial variation in pericellular rheology, we divide the field of view into different regions. The first region is a circle with radius $R_0 = 150$ pixels (approximately 23.4 μm)

https://doi.org/10.1021/acsbiomaterials.1c00871
ACS Biomater. Sci. Eng. XXXX, XXX, XXX−XXX

centered at the cell center. Each subsequent region is a ring centered at the same place. The outer radius of ring i, R_i, follows $R_i = R_{i-1} + 23.4\ \mu$m. The inner radius of the ring is the outer radius of the previous ring: R_{i-1}. The size of each ring is chosen to ensure that enough particles are in the region for accurate MPT measurements.[43,44] Figure 2 shows that these regions superimposed onto the image of the cell at the same time point on day 4 post-encapsulation. Examples of data on days 2 and 3 as well as an additional set for day 4 are provided in the Supporting Information (day 2: Figures S2 and S3, day 3: Figures S4 and S5, day 4: Figure S6). The α value of the material in each ring is represented by color with warm colors representing a gel with lower α values ($\alpha < 0.2$) and cool colors representing a sol with higher α values ($\alpha > 0.3$). The transition from gel to sol occurs when $\alpha = n$, which is represented by an orange color ($0.2 \leq n \leq 0.3$). For the untreated cell (Figure 2a–c), we measure minimal degradation at 0 min (Figure 2a), indicated by the bright red color at all distances from the cell center. At 32 and 57 min (Figure 2b,c), we measure an increase in degradation, but the material does not enter the gel–sol transition region. These results are consistent with those in Figure 1.

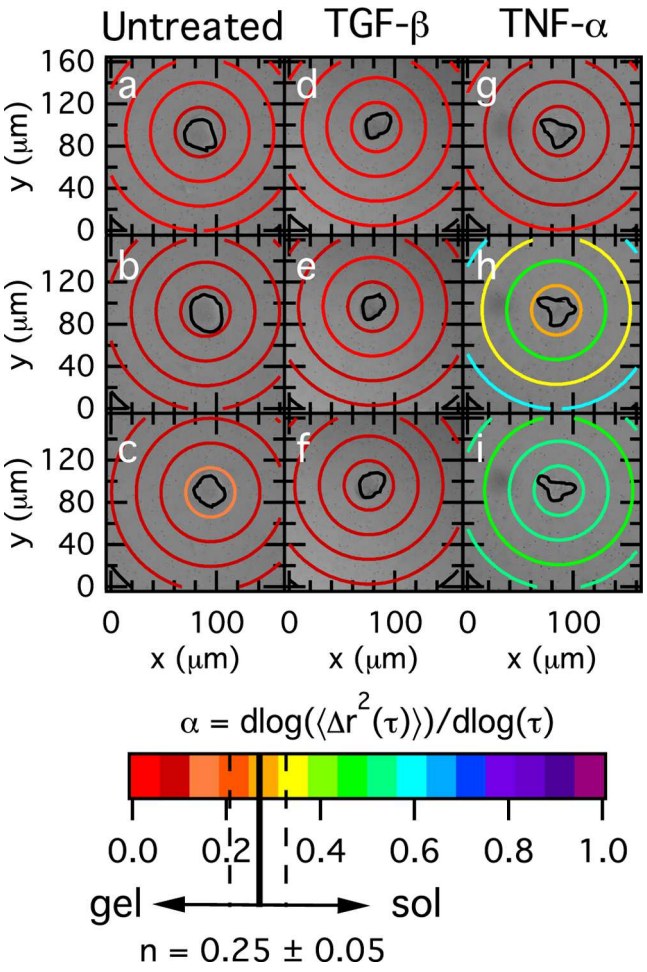

Figure 2. Spatial variation of α around three different hMSCs 4 days post-encapsulation. α is represented by color: warm colors represent gel ($\alpha < 0.2$), cool colors represent sol ($\alpha > 0.3$), and the transition region is represented by an orange color ($0.2 \leq \alpha \leq 0.3$). Each column represents a single cell in a particular treatment group: (a–c) untreated, (d–f) TGF-β, or (g–i) TNF-α treated cells. In the background of each graph is an image of the cell at that time point. Data are collected after initially locating the cell at (a) 0, (b) 32, (c) 57, (d) 0, (e) 25, (f) 50, (g) 0, (h) 19, and (i) 26 min.

The TGF-β treated cell, shown in Figure 2d–f, does less remodeling than the untreated cell. The color of each ring for the TGF-β treated cell remains red everywhere throughout the observation time, 50 min, while the untreated cell has higher α at the innermost ring in Figure 2c. These results are in agreement with the TGF-β and untreated cell data in Figure 1. The reduction in secreted MMPs and increase in TIMPs, which has been shown in the literature to be caused by incubation in TGF-β, results in minimal and spatially uniform degradation with respect to distance from the cell center.[27,34,35]

The TNF-α treated cell, shown in Figure 2g–i, begins with similar measurements to the untreated and TGF-β treated cells. At $t = 0$ min (Figure 2g), all regions around the cell are in the gel state. As time progresses to $t = 19$ min, α increases in all regions around the cell. Material immediately around the cell is in the transition region ($0.2 \leq \alpha \leq 0.3$), while regions further away have transitioned and are in the sol state. This spatial profile of degradation is consistent with previous results, which characterized this profile as a reverse reaction-diffusion degradation profile.[1,3,9] Daviran et al. found that the regions further away from the cell center ($r \geq 70.2\ \mu$m) are where the highest rate of MMP–TIMP unbinding occurs.[9] Because of this, there are more active MMPs further from the cell, resulting in scaffold degradation. In regions closer to the cell, TIMPs are bound to MMPs, inhibiting their activity resulting in minimal degradation. Despite evidence from previous studies showing TNF-α increasing the secretion of MMPs and decreasing the secretion of TIMPs, Figure 2h still has a reverse reaction-diffusion profile because TIMPs and MMPs are still present but at different concentrations than those around untreated hMSCs.[25,29,30] This changes by $t = 26$ min, where α is more uniform than at $t = 19$ min throughout the field of view with $\alpha \approx 0.5$. Since we hypothesize that there are fewer TIMPs being secreted by the hMSC because of the presence of TNF-α, more unbound and active MMPs are present throughout the field of view. This results in degradation near the cell, which is not measured at $t = 19$ min. The data in Figure 2 quantify the change in rheology around a single cell in each treatment group. To look at how α changes at each distance from the cell center on days 2–4 post-encapsulation, we plot the average α value, α_{avg}, at each distance for each treatment group in Figure 3.

On day 2 post-encapsulation (Figure 3a), we measure relatively low α_{avg} at all distances away from the cell center for all treatment groups. This is because the cells have not had a significant amount of time to remodel the pericellular region, and this results in most of the material remaining in the gel state. In all but the furthest region from the cell center, there is a significant difference in remodeling around cells treated with TGF-β and TNF-α, with α_{avg} around untreated cells. Treatment with TGF-β, which has been shown to suppress MMP secretion and, therefore, matrix degradation in previous literature, results in lower α_{avg}, which are uniform across the field of view.[27,34,35] In contrast, TNF-α treatment which previous reports show increases the production of MMPs and decreases TIMPs results in more scaffold degradation and higher α_{avg} values at all distances up to 93.6 μm from the cell center.[25,28−30,32] Additionally, the standard deviation in α for the TNF-α treatment group is approximately 60% higher than the untreated group. This larger spread in the α values for

https://doi.org/10.1021/acsbiomaterials.1c00871
ACS Biomater. Sci. Eng. XXXX, XXX, XXX–XXX

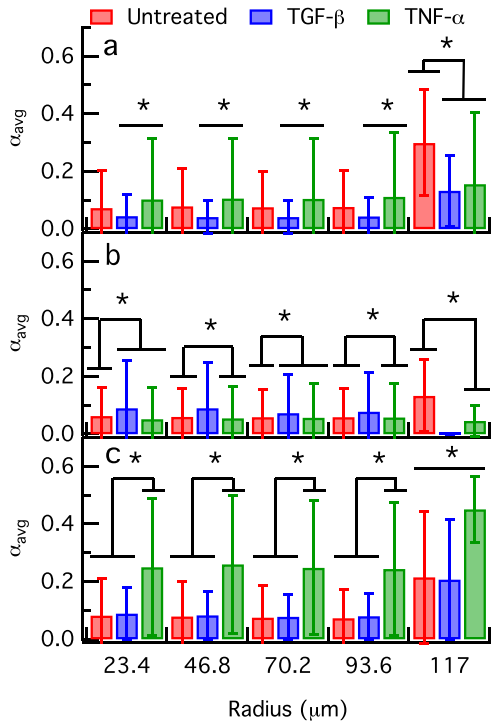

Figure 3. α_{avg} for all samples in a given treatment group on days (a) 2, (b) 3, and (c) 4 post-encapsulation. Each bar represents α_{avg} for materials at a particular distance from the cell center. The data are grouped by post-encapsulation day and the treatment group with red representing untreated, blue representing TGF-β treated, and green representing TNF-α treated cells. Error bars represent the standard deviation. *$p < 0.05$.

TNF-α treated hMSCs suggests that increased MMP activity creates more heterogeneity in the rheology of the pericellular region, which agrees with spatial maps in Figure 2g–i. In general, day 2 post-encapsulation results agree well with those from Figure 1a, with most distances measured with $\alpha_{avg} < n$.

For each treatment group on day 2 post-encapsulation, the region furthest from the cell center has statistically significantly higher α_{avg} than all other regions. $R = 117$ μm is the distance which previous studies have shown has high MMP–TIMP unbinding, which leads to more active MMPs resulting in a more degraded structure.[9] The only exception is when comparing the regions 93.6 and 117 μm away from TNF-α treated cells, where no statistically significant difference is measured between the values of α_{avg}. Because literature has shown that TNF-α decreases TIMPs and increases MMPs, we hypothesize that α_{avg} will be similar at 93.6 and 117 μm away from TNF-α treated cells because there will be more active MMPs closer to the cell center resulting in these regions having similar degradation. It should be noted that the furthest region measured, $R = 117$ μm, has significantly fewer measurements than the other regions. Additionally, the values for α_{avg} for untreated cells on days 2 and 3 at 117 μm from the cell center are within error of one another, as well as, the values for TNF-α treated cells. During MPT measurements, only material up to approximately 80 μm away from the cell center can be seen when the cell is centered in the field of view at $t = 0$ min. As the cell moves in the x–y plane, material further from its center can be characterized. Because the cell needs to move significantly in the x–y plane for this region to be included in the field of view, fewer samples are measured in this region. Because of this, an average of only 19 samples is measured at $R = 117$ μm for each treatment group on each day compared to all other regions, which each have an average of 263 samples for each treatment group on each day.

On day 3 post-encapsulation (Figure 3b), we continue to measure different degrees of remodeling at different distances from the cell center based on the treatment group. TGF-β treated cells have statistically significant higher α_{avg} values at 23.4 and 70.2 μm than untreated cell-mediated degradation. While this difference is small, it is still statistically significant and will be discussed with Figure 4, where the full distribution

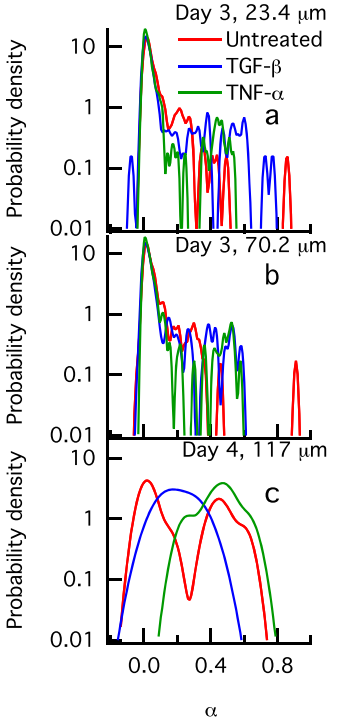

Figure 4. Three probability distributions of α values around cells from Figure 3: (a) day 3 at 23.4 μm, (b) day 3 at 70.2 μm, and (c) day 4 at 117 μm. In (a) and (b), the α distribution around untreated cells is statistically different from each of the α distributions around TGF-β and TNF-α treated cells ($p < 0.05$). In (c), all three distributions are different from one another ($p < 0.05$). All distributions for all days post-encapsulation and all distances from the cell center are available in the Figure S7, Supporting Information.

of α in this region is shown. This difference may be due to an increase in actin stress fiber formation. A previous study found that treatment of epithelial cells with TGF-β induces actin stress fibers and upregulates the expression of actin-binding proteins.[69] An increase in actin-binding proteins in our hMSCs would cause motile cells treated with TGF-β to exert more force on their surrounding material to remodel and migrate. This would result in an increase in probe mobility around TGF-β treated hMSCs in regions close to the cell center. TNF-α treated cells have statistically different distributions of α_{avg} from untreated cells at all distances from the cell center. This is likely due to increased heterogeneity in the scaffold structure around hMSCs treated with TNF-α. This agrees with data provided in Figure 2h,i, which shows significant variation in α with respect to distance from the cell center around the TNF-α treated cell. Finally, no data is collected at 117 μm for TGF-β

https://doi.org/10.1021/acsbiomaterials.1c00871
ACS Biomater. Sci. Eng. XXXX, XXX, XXX–XXX

treated cells as none of these cells moved far enough in the field of view for this region to be visible.

On day 4 post-encapsulation (Figure 3c), α_{avg} for all treatment groups is statistically different relative to previous days. Notably, on day 4, there is a statistically significant higher α_{avg} in regions around cells treated with TNF-α than those same regions around untreated and TGF-β treated cells. This is likely due to increased MMP secretions, which TNF-α has previously been reported to cause.[25,28−30,32] At 117 μm, all three α_{avg} are different from one another. Similar to previous days, this may be due to the fact that regions further away from the cell are where TIMPs unbind from MMPs.[1,3,9] This region also has less data (average of 15 measurements for all treatment groups at 117 μm compared to 279 measurements at 23.4−93.6 μm). The amount of data in each population being compared has a direct impact on the outcome of a statistical hypothesis test, and in this situation where the two populations have such different sizes, it may contribute to the statistically significant differences between the treatment groups. The differences between each treatment group show how the presence of cytokines in the pericellular region impacts hMSC-mediated material remodeling. TGF-β and TNF-α have been shown in previous literature to change the secretion of MMPs and TIMPs; the concentration of these molecules affects the degree the surrounding material is degraded.[25,27−30,32,34,35] Exposure to each cytokine in the fluid environment will therefore change pericellular rheology since TNF-α increases remodeling by hMSCs due to increased enzymatic activity and TGF-β decreases remodeling by hMSCs due to a decrease in enzymatic activity.[25,27−30,32,34,35] Some of the differences between treatment groups may not be entirely clear in Figure 3. Therefore, we also present probability distribution functions of α values in Figure 4 to better understand the differences measured in α_{avg} values.

Figure 4 shows probability distribution functions (PDFs) in α used to calculate data presented in Figure 3 for 23.4 and 70.2 μm on day 3 (Figure 4a,b) and 117 μm on day 4 post-encapsulation (Figure 4c). These distributions show how α varies at a particular distance for different cells on a given day. A peak at $\alpha = 0$ indicates that most of the cells have no degraded material at this distance, while higher α values indicate more hMSC-mediated degradation in these regions. Distributions for all distances from the cell center on all days are available in the Supporting Information (Figure S7).

We will begin our discussion with day 3 post-encapsulation. Figure 4a,b shows that all cells have a peak at $\alpha = 0$ with a distribution skewed toward higher α. The peak at $\alpha = 0$ indicates that the material is a gel because cells have not degraded at this distance, and the skewness toward higher α is a result of more material remodeling by hMSC-secreted MMPs. At 23.4 μm from the cell center, Figure 4a, the scaffold in the pericellular region is mostly in the gel phase. At this distance from the cell center, there are not many active MMPs due to TIMPs binding to them immediately after secretion and preventing their activity.[1,3,9] The distribution of α around untreated cells is skewed slightly to the right due to TIMPs not binding all secreted MMPs leaving some free MMPs to degrade the material and cytoskeletal tension reversibly remodeling the scaffold. The distribution of α around TGF-β treated cells is concentrated more tightly around $\alpha \to 0$. TGF-β, which previous work has shown increases the production of TIMPs, creates more TIMPs to bind secreted MMPs immediately around the cell, causing more cells to be in gelled material.[27,34,35] This results in a statistically significant difference between the α distributions for the untreated and TGF-β treatment groups at this distance. Additionally, there are smaller peaks at higher α values for the α distribution around TGF-β treated cells at 23.4 μm from the cell center. This may be due to an increase in filamentous actin in the cytoskeleton of the hMSC. Previous reports show that long-term (≈48 h) exposure of human prostate cancer cells to TGF-β-induced membrane ruffles formed actin stress fibers.[70] An increase in actin would enable the hMSC to apply force to the network and reversibly remodel material more easily as it migrates. This results in increased remodeling where cells apply cytoskeletal tension to the network. We hypothesize that a similar situation is occurring in Figure 4b, which is data for day 3 post-encapsulation at 70.2 μm. More TIMPs are available to bind MMPs, causing the α distribution around TGF-β treated cells to be more concentrated around $\alpha \to 0$, resulting in a difference between the two treatment groups.

The α distributions around TNF-α treated cells in Figure 4a,b also have a peak at $\alpha = 0$ because the material around most cells at these distances tends not to be degraded. By day 3 post-encapsulation, most cells have not remodeled past the gel−sol transition because cell-secreted MMPs have not had enough time to break cross-links. This agrees with data shown in Figure 1. There are some cells treated with TNF-α which have degraded these regions, which are shown by the skewness to $\alpha \approx 0.4$, the second peak of each α distribution around TNF-α treated cells in Figure 4a,b. These regions are degraded because of the increase in MMPs and decrease in TIMPs, which TNF-α has been shown in previous reports to cause in hMSCs.[25,28−30,32] We attribute the statistically significant difference between the α distributions around TNF-α treated and untreated cells to the difference in skewness between them caused by the change in hMSC secretions changing the degradation in these regions.

Figure 4c shows PDFs in α for 117 μm away from the cell center for all three treatment groups on day 4 post-encapsulation. The distribution for untreated cells has two peaks, one at $\alpha \approx 0$ and the other at $\alpha \approx 0.5$. This indicates that two distinct populations of untreated cells exist, producing two peaks in the distribution. The peak at $\alpha \approx 0$ is from hMSCs that have not degraded their microenvironment at this distance. The peak at $\alpha \approx 0.5$ is from cells that have degraded their microenvironment past the gel−sol transition at this distance from the cell center. The distribution of α around TNF-α treated cells at this distance is concentrated at higher α values with a single peak around $\alpha \approx 0.5$. Notably, nearly the entire distribution is above the gel−sol transition, $\alpha > n = 0.25 \pm 0.05$. Since this region has the greatest rate of MMP−TIMP unbinding and TNF-α has been shown in the literature to increase MMP-mediated remodeling, it shifts the distribution to higher α, which are above the gel−sol transition.[25,28−30,32] When comparing α distributions around untreated cells and TNF-α treated cells, the differences become more evident. The right peak in α measured around untreated cells is similar to the one created by TNF-α treated cells. This is because in this region, around untreated cells, MMPs unbind from TIMPs, resulting in scaffold degradation. The increase in MMP secretions caused by TNF-α and decrease in TIMP secretions results in a single peak for the distribution of α around TNF-α treated cells, where all cells have degraded the material at this distance. Due to this, we measure a similar distribution of α between untreated and TNF-α treatment groups at this

https://doi.org/10.1021/acsbiomaterials.1c00871
ACS Biomater. Sci. Eng. XXXX, XXX, XXX−XXX

distance. The α distribution around TGF-β treated cells is different from the other two. It has a single peak at $\alpha \approx 0.17$, indicating that the material is mostly in the gel state or transitional region. We hypothesize that this region is less degraded despite the increase in MMP−TIMP unbinding because of the increase of TIMPs and decrease of MMPs, which previous literature has shown TGF-β causes.[27,34,35] We hypothesize that if given enough time, the α distribution around TGF-β treated cells would transition to a sol as the reduced number of MMPs are allowed to continue to degrade the scaffold.

Now that we have shown how cells in each treatment group remodel their microenvironment, we describe cell motility. Figure 5 shows distributions of cell speeds as a function of the

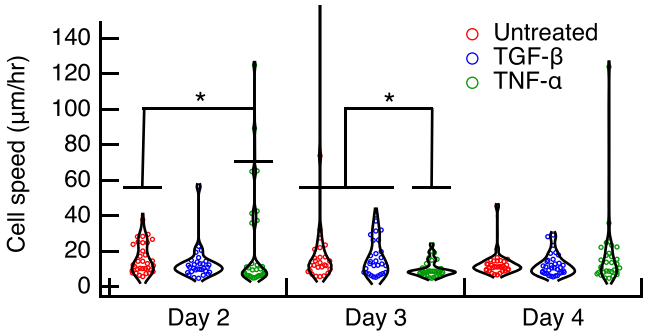

Figure 5. Cell speed for each treatment group on each day. Each marker represents the average speed of a single cell calculated by averaging the speed of each step, v_{step}, using eq 3. A single outlier is present 3 days post-encapsulation for a control cell, which is outside the range of the y-axis, which is cut so that the data is more visible. This graph is reproduced with all data shown in the Supporting Information (Figure S8). *$p < 0.05$.

treatment group and post-encapsulation day. The average speed of each treatment group is similar on all days post-encapsulation. Most cells have speeds between 0 and 40 μm h^{-1}. We measure statistically significant differences between the speeds of TNF-α treated cells and untreated cells on day 2 post-encapsulation. On this day, most cells that are untreated or treated with TNF-α have cell speeds between 10 and 20 μm h^{-1}. A few TNF-α treated cells have significantly higher speeds, upwards of 40 μm h^{-1}. We attribute the difference in these distributions to the fast-moving TNF-α treated cells which have quickly remodeled their surroundings due to an increase in MMP secretions and decrease in TIMP secretions, which TNF-α has been shown to cause in previously published results.[25,28−30,32] Statistical significance in cell speed is also measured between TNF-α treated cells and both untreated and TGF-β treated cells on day 3 post-encapsulation, with the TNF-α treatment group having more cells concentrated at lower speeds than the TGF-β treatment group.

We attribute these differences in speed to changes in cellular secretions caused by the presence of cytokines in the fluid environment. These changes in secretions change pericellular rheology, which correlates with cellular speed.[11] Figure 3a shows that TNF-α has a higher α_{avg} than untreated cells on day 2 post-encapsulation. This correlates with a higher average speed measured for TNF-α treated cells on day 2 post-encapsulation in Figure 5. The results from these two figures agree and indicate that cells that remodel their microenvironment more have higher cell speeds. Similarly, on day 3, each treatment group has a similar α_{avg} and all cell speeds are ≈10−30 μm h^{-1}.

On day 4 post-encapsulation, we measure no statistical significance between cell speeds of each treatment group. From Figure 3c, TGF-β treated and untreated cells have similar pericellular α_{avg} values on day 4 post-encapsulation, and we also measure that they have similar cell speeds, Figure 5. While the α_{avg} value around TNF-α treated cells is significantly higher on day 4 than other treatment groups, cell speed remains comparable with the other two groups. This may be because by day 4, cells treated with TNF-α have degraded their surroundings and are not able to effectively attach to the network, limiting their migration. Cell migration persistence is also important for determining if hMSCs are migrating effectively. If cells are not persistent, they are less likely to migrate out of the hydrogel and into the wound. To measure the impact of cytokines on hMSC persistence, we quantify persistence by measuring the cosine of the angle between subsequent cell displacements and relate it to pericellular rheology.

In addition to affecting how hMSCs remodel their surroundings, cytokines are also responsible for directing hMSCs to the wounded area by a concentration gradient.[14] hMSCs receive these cues and migrate up the gradient from regions of low concentration far from the wound to regions of higher concentration at the wound. Our future experiments will provide gradients in cytokines, but the present experiments provide cyotkines isotropically in the incubation fluid. In order for cells to be motile and persistent, they must degrade their microenvironment, and this degradation is altered by cytokines through their effects on MMP and TIMP secretions. Additionally, we are studying two cytokines that occur at significantly different times during the wound healing process: TNF-α which is present early in the healing process when hMSCs may not be present at the wound and TGF-β which is present when the wound is entering its later stages of healing and hMSCs are coordinating the process. Because of this, we hypothesize that TNF-α will increase cellular persistence because it increases remodeling by hMSCs. Cells in more remodeled microenvironments will be able to move more freely through their surroundings since there is less structure and will, therefore, be more persistent. Conversely, we also hypothesize that treatment with TGF-β will not significantly improve the persistence of cells because it encourages the formation of new matrix, preventing cells from being able to remodel and migrate freely within our scaffold. We quantify persistence by calculating the cosine of the angle between cell displacements, $\cos\theta$. Values of $\cos\theta$ near 1 indicate that cell displacements occur relatively in line with one another and that the cell is persistent. Values of $\cos\theta$ that are much less than 1 or negative indicate that the cell is moving randomly and is not persistent.

Figure 6 shows the PDFs of $\cos\theta$ with respect to α. After three measurements are made of a given cell, a dot product is calculated from the resultant two displacements and $\cos\theta$ is calculated using eq 4. This value of $\cos\theta$ is paired with the last α value of the three measured time points $\alpha(t_3)$ into a single point: $(\alpha(t_3), \cos\theta)$. Here, α is determined from all particles in the entire field of view. The calculation is repeated using cell positions at t_i, t_{i+1}, and t_{i+2} until each cell location has been used to calculate a $\cos\theta$. Only values of $\cos\theta$ whose two vectors have an average magnitude greater than 1 μm are considered in Figure 6. This is done to prevent calculating

https://doi.org/10.1021/acsbiomaterials.1c00871
ACS Biomater. Sci. Eng. XXXX, XXX, XXX−XXX

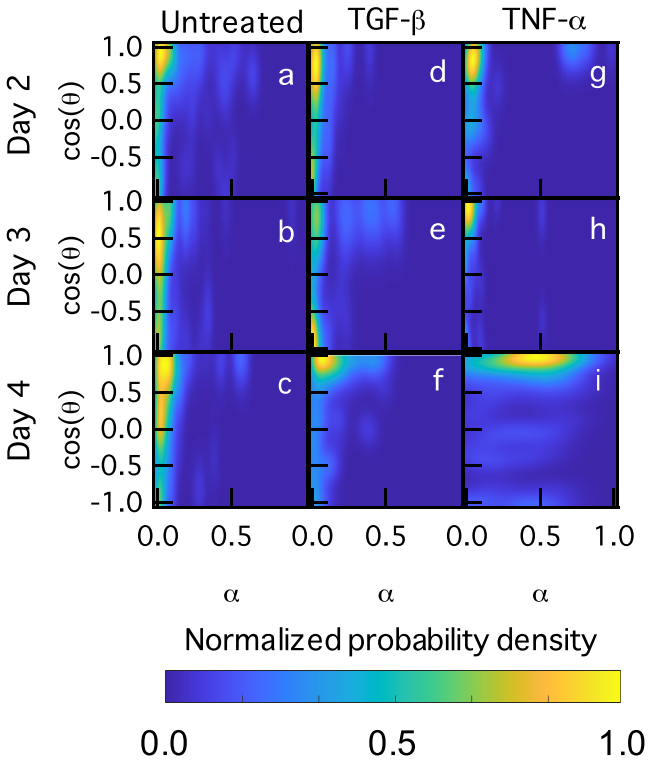

Figure 6. Persistence of hMSCs measured as $\cos\theta$ *vs* α for all treatment groups ((a−c) untreated, (d−f) TGF-β, and (g−i) TNF-α treated cells) on (a, d, g) days 2, (b, e, h) 3, and (c, f, i) 4 post-encapsulation. Data are presented as a smoothed probability density function with yellow and orange representing high probability and blue and green representing lower probability. Probability is normalized by the maximum probability in that image to enable comparison between images.

$\cos\theta$ for cells that are not moving, where the measured change of cell displacement will be within the error of accuracy of the cell center identification. Each point is grouped by post-encapsulation day and the treatment group. These points for each treatment group and post-encapsulation day are then used to calculate the PDFs in Figure 6.

On day 2 post-encapsulation (Figure 6a,d,g), we measure that most samples have α values close to zero, which is expected since the cells were recently encapsulated and have not had time to remodel their microenvironment. The peak of the probability distribution is concentrated at high $\cos\theta$ and low α for all treatment groups. This indicates that in material which is not degraded, most cells are persistent with high $\cos\theta$, but many cells are also not persistent. For each distribution, there are also some higher α values. These high values result in $\cos\theta$ values closer to 1. This is shown by the light blue at high $\cos\theta$ and α. This indicates that environments that are remodeled lead to cells that have more persistent displacements. As the material is remodeled by hMSCs, their ability to migrate is easier and they start to migrate in a single direction. They may also be following previously degraded paths in the material, which are easier to degrade further and migrate through.

Day 3 post-encapsulation PDFs (Figure 6b,e,h) have similar trends to day 2 with distributions concentrated at low α values. $\cos\theta$ is concentrated at ≈0.8 for untreated cells and is fairly uniform for TGF-β treated cells and concentrated at ≈0.8 for TNF-α treated cells. Measurements at higher α values correspond to higher $\cos\theta$ for untreated and TGF-β treated cells. At high $\cos\theta$, the distribution for TGF-β treated cells reaches higher α values near $\alpha \approx 0.5$. We hypothesize that the increase in filamentous actin as well as increased remodeling by day 3 for hMSCs treated with TGF-β enables some cells to be more persistent in this treatment group.[69] TNF-α treated cell measurements become more concentrated at high $\cos\theta$ than on day 2 because these cells have had more time in the hydrogel and are beginning to degrade and migrate through the scaffold.

On day 4 post-encapsulation (Figure 6c,f,i), we continue to measure that most samples for untreated and TGF-β treated cells have $\alpha < n$, which is the same as the results given in Figure 3c. When $\alpha > n$, cells tend to have more persistent migration with $\cos\theta \to 1$. This is shown in the untreated group (Figure 6c), where a population is shown having $\alpha \approx 0.6$ and $\cos\theta \approx 0.8$. In the TGF-β treatment group (Figure 6f), there is a tail extending from the peak of the distribution at $\alpha \approx 0.1$ and $\cos\theta \approx 1$ toward $\alpha \approx 0.4$ at high values of $\cos\theta$. In TNF-α treated cells on this day, the primary peak of the PDF has $\alpha \approx 0.4$ and $\cos\theta \approx 0.8$, indicating that most cells which have degraded their material past the gel−sol transition region are highly persistent. These results show that hMSCs which are encapsulated in a gel are not persistent. Once an hMSC has remodeled its surroundings to a sol, it will tend to migrate in a straight path and be persistent. The increased persistence of TNF-α treated hMSCs can occur in part due to the increased secretion of MMPs and reduced secretion of TIMPs, which TNF-α has been shown to cause in previous reports.[25,28−30,32] These conditions result in increased remodeling, making the surrounding material easier to migrate through since there are fewer cross-links present to impede cell motility. This allows the cell to migrate persistently. Additionally, as hMSCs are migrating in the scaffold by day 4, they may migrate through paths already degraded in the material, which will result in higher persistence.

The results in Figure 6 show that hMSCs in more remodeled environments ($\alpha > n$) migrate in a more persistent manner, while those surrounded by the gel ($\alpha < n$) migrate more randomly. Additionally, cells that remodel more readily, such as those treated with TNF-α, are more persistent by day 4 due to their enhanced ability to degrade material prior to migration and the cumulative effect of the previous degradation of the material. We hypothesize that significant persistent migration would occur if cytokines are presented to cells in a concentration gradient mimicking the *in vivo* environment during the wound healing process.

CONCLUSIONS

In this work, we characterize spatiotemporal remodeling of the pericellular region by migrating hMSCs in response to TGF-β and TNF-α provided in the fluid environment. We measure that TGF-β treated cells remodel their surroundings less than TNF-α treated cells. This is due to the effects each cytokine has been shown to have on hMSC secretions in various previous studies.[25,27−30,32,34,35] TGF-β encourages the formation of new matrix by decreasing the production of MMPs and increasing the production of their inhibitors, TIMPs, which decreases matrix degradation. By contrast, TNF-α encourages degradation and remodeling by increasing MMP secretions and decreasing TIMP secretions. We characterize spatial changes in pericellular rheology around encapsulated cells and find that the presence of cytokines impacts this

https://doi.org/10.1021/acsbiomaterials.1c00871
ACS Biomater. Sci. Eng. XXXX, XXX, XXX−XXX

remodeling. We measure that the region with the highest MMP−TIMP unbinding has significant differences between each treatment group attributed to the presence of these cytokines and their effects on the concentrations of MMPs and TIMPs.[9,14] Additionally, we measure that cells that have degraded past the gel−sol transition have more persistent migration, while those that have not degraded past the gel−sol transition migrate randomly. This directly links the rheology of the pericellular region to cell persistence.

The results of this work are important for the design and use of implantable wound healing scaffolds because knowing how hMSCs will remodel the scaffold in the presence of cytokines will provide a better understanding of how these materials will function *in vivo*. Additionally, it may lead to the design of more complex materials, which present cytokines to hMSCs to instruct cell function toward the goal of enhanced cell delivery and a resolved wound.

■ ASSOCIATED CONTENT

Supporting Information

The Supporting Information is available free of charge at https://pubs.acs.org/doi/10.1021/acsbiomaterials.1c00871.

Additional data for α *vs* time; additional degradation profiles on days 2−4 post-encapsulation; the distribution of α around cells from each treatment condition at each distance from the cell center; complete cell speed data (PDF)

■ AUTHOR INFORMATION

Corresponding Author

Kelly M. Schultz − *Department of Chemical and Biomolecular Engineering, Lehigh University, Bethlehem, Pennsylvania 18015, United States;* orcid.org/0000-0001-9040-126X; Phone: 01 610 758 2012; Email: kes513@lehigh.edu

Authors

Maryam Daviran − *Department of Chemical and Biomolecular Engineering, Lehigh University, Bethlehem, Pennsylvania 18015, United States*

John A. McGlynn − *Department of Chemical and Biomolecular Engineering, Lehigh University, Bethlehem, Pennsylvania 18015, United States*

Jenna A. Catalano − *Department of Chemical and Biomolecular Engineering, Lehigh University, Bethlehem, Pennsylvania 18015, United States*

Hannah E. Knudsen − *Department of Chemical and Biomolecular Engineering, Lehigh University, Bethlehem, Pennsylvania 18015, United States*

Kilian J. Druggan − *Department of Chemical and Biomolecular Engineering, Lehigh University, Bethlehem, Pennsylvania 18015, United States*

Kiera J. Croland − *Department of Chemical and Biomolecular Engineering, Lehigh University, Bethlehem, Pennsylvania 18015, United States*

Amanda Stratton − *Department of Bioengineering, Lehigh University, Bethlehem, Pennsylvania 18015, United States*

Complete contact information is available at: https://pubs.acs.org/10.1021/acsbiomaterials.1c00871

Author Contributions

§M.D. and J.A.M. contributed equally to this work.

Notes

The authors declare no competing financial interest.

■ ACKNOWLEDGMENTS

Funding for this work was provided in part by the National Science Foundation under Grant no. CBET-1751057. Research reported in this publication was supported in part by the National Institute of General Medical Sciences of the National Institutes of Health under Award Number R15GM119065. The content is solely the responsibility of the authors and does not necessarily represent the official views of the National Institutes of Health.

■ REFERENCES

(1) Daviran, M.; Schultz, K. M. Characterizing the Dynamic Rheology in the Pericellular Region by Human Mesenchymal Stem Cell Re-engineering in PEG-Peptide Hydrogel Scaffolds. *Rheol. Acta* **2019**, *58*, 421−437.

(2) Mazzeo, M. S.; Chai, T.; Daviran, M.; Schultz, K. M. Characterization of the Kinetics and Mechanism of Degradation of Human Mesenchymal Stem Cell-Laden Poly(ethylene glycol) Hydrogels. *ACS Appl. Bio Mater.* **2019**, *2*, 81−92.

(3) Daviran, M.; Longwill, S. M.; Casella, J. F.; Schultz, K. M. Rheological Characterization of Dynamic Remodeling of the Pericellular Region by Human Mesenchymal Stem Cell-Secreted Enzymes in Well-Defined Synthetic Hydrogel Scaffolds. *Soft Matter* **2018**, *14*, 3078−3089.

(4) Schultz, K. M.; Kyburz, K. A.; Anseth, K. S. Measuring Dynamic Cell-Material Interactions and Remodeling During 3D Human Mesenchymal Stem Cell Migration in Hydrogels. *Proc. Natl. Acad. Sci. U.S.A.* **2015**, *112*, E3757−E3764.

(5) Kyburz, K. A.; Anseth, K. S. Three-Dimensional hMSC Motility Within Peptide-Functionalized PEG-Based Hydrogels of Varying Adhesivity and Crosslinking Density. *Acta Biomater.* **2013**, *9*, 6381−6392.

(6) Guvendiren, M.; Burdick, J. A. Engineering Synthetic Hydrogel Microenvironments to Instruct Stem Cells. *Curr. Opin. Biotechnol.* **2013**, *24*, 841−846.

(7) Lutolf, M. P.; Lauer-Fields, J. L.; Schoekel, H. G.; Metters, A. T.; Weber, F. E.; Fields, G. B.; Hubbell, J. A. Synthetic Matrix Metalloproteinase-Sensitive Hydrogels for the Conduction of Tissue Regeneration: Engineering Cell-Invasion Characteristics. *Proc. Natl. Acad. Sci. U.S.A.* **2003**, *100*, 5413−5418.

(8) Daviran, M.; Catalano, J.; Schultz, K. M. Determining How Human Mesenchymal Stem Cells Change their Degradation Strategy in Response to Microenvironmental Stiffness. *Biomacromolecules* **2020**, 3056−3068.

(9) Daviran, M.; Caram, H. S.; Schultz, K. M. Role of Cell-Mediated Enzymatic Degradation and Cytoskeletal Tension on Dynamic Changes in the Rheology of the Pericellular Region Prior to Human Mesenchymal Stem Cell Motility. *ACS Biomater. Sci. Eng.* **2018**, *4*, 468−472.

(10) Tibbitt, M. W.; Anseth, K. S. Hydrogels as extracellular matrix mimics for 3D cell culture. *Biotechnol. Bioeng.* **2009**, *103*, 655−663.

(11) McGlynn, J. A.; Druggan, K. J.; Croland, K. J.; Schultz, K. M. Human mesenchymal stem cell-engineered length scale dependent rheology of the pericellular region measured with bi-disperse multiple particle tracking microrheology. *Acta Biomater.* **2020**, 405−417.

(12) Thapa, R. K.; Margolis, D. J.; Kiick, K. L.; Sullivan, M. O. Enhanced wound healing via collagen-turnover-driven transfer of PDGF-BB gene in a murine wound model. *ACS Appl. Bio Mater.* **2020**, *3*, 3500−3517.

(13) Lutolf, M. P.; Weber, F. E.; Schmoekel, H. G.; Schense, J. C.; Kohler, T.; Muller, R.; Hubbell, J. A. Repair of Bone Defects Using Synthetic Mimetics of Collagenous Extracellular Matrices. *Nat. Biotechnol.* **2003**, *21*, 513−518.

(14) Maxson, S.; Lopez, E. A.; Yoo, D.; Danilkovitch-Miagkova, A.; LeRoux, M. A. Concise Review: Role of Mesenchymal Stem Cells in Wound Repair. *Stem Cells Transl. Med.* **2012**, *1*, 142−149.
(15) Deans, R. J.; Moseley, A. B. Mesenchymal stem cells: Biology and potential clinical uses. *Exp. Hematol.* **2000**, *28*, 875−884.
(16) Nombela-Arrieta, C.; Ritz, J.; Silbersyein, L. E. The elusive nature and function of mesenchymal stem cells. *Nat. Rev. Mol. Cell Biol.* **2011**, *12*, 126−131.
(17) Shi, Y.; Su, J.; Roberts, A. I.; Shou, P.; Rabson, A. B.; Ren, G. How mesenchymal stem cells interact with tissue immune responses. *Trends Immunol.* **2012**, *33*, 136−143.
(18) Jackson, W. M.; Nesti, L. J.; Tuan, R. S. Mesenchymal stem cell therapy for attenuation of scar formation during wound healing. *Stem Cell Res. Ther.* **2012**, *3*, No. 20.
(19) Eggenhofer, E.; Luk, F.; Dahlke, M. H.; Hoogduijn, M. J. The life and fate of mesenchymal stem cells. *Front. Immunol.* **2014**, *5*, No. 148.
(20) Otero-Viñas, M.; Falanga, V. Mesenchymal Stem Cells in Chronic Wounds: The Spectrum from Basic to Advanced Therapy. *Adv. Wound Care* **2016**, 149−163.
(21) Jeon, O.; Alt, D. S.; Linderman, S. W.; Alsberg, E. Biochemical and physical signal gradients in hydrogels to control stem cell behavior. *Adv. Mater.* **2013**, *25*, 6366−6372.
(22) Hafner, J.; Grijalva, D.; Ludwig-Husemann, A.; Bertels, S.; Bensinger, L.; Raic, A.; Gebauer, J.; Oelschlaeger, C.; Bastmeyer, M.; Bieback, K.; Lee-Thedieck, C.; Willenbacher, N. Monitoring matrix remodeling in the cellular microenvironment using microrheology for complex cellular systems. *Acta Biomater.* **2020**, *111*, 254.
(23) Fakhouri, A. S.; Weist, J. L.; Tomusko, A. R.; Leight, J. L. High-Throughput Three-Dimensional Hydrogel Cell Encapsulation Assay for Measuring Matrix Metalloproteinase Activity. *Assay Drug Dev. Technol.* **2019**, *17*, 100−115.
(24) Leight, J. L.; Alge, D. L.; Maier, A. J.; Anseth, K. S. Direct Measurement of Matrix Metalloproteinase Activity in 3D Cellular Microenvironments Using a Fluorogenic Peptide Substrate. *Biomaterials* **2013**, *34*, 7344−7352.
(25) Barrientos, S.; Stojadinovic, O.; Golinko, M. S.; Brem, H.; Tomic-Canic, M. Growth factors and cytokines in wound healing. *Wound Repair Regener.* **2008**, *16*, 585−601.
(26) Singer, A. J.; Clark, R. A. Cutaneous Wound Healing. *N. Engl. J. Med.* **1999**, *341*, 738−746.
(27) Overall, C.; Wrana, J.; Sodek, J. Transcriptional and post-transcriptional regulation of 72-kDa gelatinase/type IV collagenase by transforming growth factor-beta 1 in human fibroblasts. Comparisons with collagenase and tissue inhibitor of matrix metalloproteinase gene expression. *J. Biol. Chem.* **1991**, *266*, 14064−14071.
(28) Shubayev, V. I.; Angert, M.; Dolkas, J.; Campana, W. M.; Palenscar, K.; Myers, R. R. TNFα-induced MMP-9 promotes macrophage recruitment into injured peripheral nerve. *Mol. Cell. Neurosci.* **2006**, *31*, 407−415.
(29) So, T.; Ito, A.; Sato, T.; Mori, Y.; Hirakawa, S. Tumor Necrosis Factor-α Stimulates the Biosynthesis of Matrix Metafloproteinases and Plasminogen Activator in Cultured Human Chorionic Cells. *Biol. Reprod.* **1992**, *46*, 772−778.
(30) Rawdanowicz, T.; Hampton, A.; Nagase, H.; Woolley, D.; Salamonsen, L. Matrix metalloproteinase production by cultured human endometrial stromal cells: identification of interstitial collagenase, gelatinase-A, gelatinase-B, and stromelysin-1 and their differential regulation by interleukin-1 alpha and tumor necrosis factor-alpha. *J. Clin. Endocrinol. Metab.* **1994**, *79*, 530−536.
(31) Engler, A. J.; Sen, S.; Lee Sweeney, H.; Discher, D. E. Matrix Elasticity Directs Stem Cell Lineage Specification. *Cell* **2006**, *126*, 677−689.
(32) Ries, C.; Egea, V.; Karow, M.; Kolb, H.; Jochum, M.; Neth, P. MMP-2, MT1-MMP, and TIMP-2 are essential for the invasive capacity of human mesenchymal stem cells: differential regulation by inflammatory cytokines. *Blood* **2007**, *109*, 4055−4063.
(33) Robson, M. C. The role of growth factors in the healing of chronic wounds. *Wound Repair Regener.* **1997**, *5*, 12−17.
(34) White, L. A.; Mitchell, T. I.; Brinckerhoff, C. E. Transforming growth factor β inhibitory element in the rabbit matrix metalloproteinase-1 (collagenase-1) gene functions as a repressor of constitutive transcription. *Biochim. Biophys. Acta, Gene Struct. Expression* **2000**, *1490*, 259−268.
(35) Zeng, G.; Mccue, H. M.; Mastrangelo, L.; Millis, A. J. Endogenous TGF-β activity is modified during cellular aging: effects on metalloproteinase and TIMP-1 expression. *Exp. Cell Res.* **1996**, *228*, 271−276.
(36) McCall, J. D.; Luoma, J. E.; Anseth, K. S. Covalently tethered transforming growth factor beta in PEG hydrogels promotes chondrogenic differentiation of encapsulated human mesenchymal stem cells. *Drug Delivery Transl. Res.* **2012**, *2*, 305−312.
(37) Anderson, S. B.; Lin, C.-C.; Kuntzler, D. V.; Anseth, K. S. The Performance of Human Mesenchymal Stem Cells Encapsulated in Cell-Degradable Polymer-Peptide Hydrogels. *Biomaterials* **2011**, *32*, 3564−3574.
(38) Weber, L. M.; Lopez, C. G.; Anseth, K. S. Effects of PEG hydrogel crosslinking density on protein diffusion and encapsulated iselt survival and function. *J. Biomed. Mater. Res., Part A* **2008**, *90A*, 720−729.
(39) Tse, J. R.; Engler, A. J. Stiffness Gradients Mimicking In Vivo Tissue Variation Regulate Mesenchymal Stem Cell Fate. *PLoS One* **2011**, *6*, No. e15978.
(40) Vincent, L. G.; Choi, Y. S.; Alonso-Latorre, B.; del Álamo, J. C.; Engler, A. J. Mesenchymal Stem Cell Durotaxis Depends on Substrate Stiffness Gradient Strength. *Biotechnology* **2013**, *8*, 472−484.
(41) Cosson, S.; Kobel, S. A.; Lutolf, M. P. Capturing complex protein gradients on biomimetic hydrogels for cell-based assays. *Adv. Funct. Mater.* **2009**, *19*, 3411−3419.
(42) Park, J. Y.; Hwang, C. M.; Lee, S. H.; Lee, S.-H. Gradient generation by an osmotic pump and the behavior of human mesenchymal stem cells under the fetal bovine serum concentration gradient. *Lab Chip* **2007**, *7*, 1673−1680.
(43) McGlynn, J. A.; Wu, N.; Schultz, K. M. Multiple Particle Tracking Microrheological Characterization: Fundamentals, Emerging Techniques and Applications. *J. Appl. Phys.* **2020**, *127*, No. 201101.
(44) Furst, E. M.; Squires, T. M. *Microrheology*, 1st ed.; Oxford University Press: New York, NY, 2017.
(45) Schultz, K. M.; Furst, E. M. Microrheology of Biomaterial Hydrogelators. *Soft Matter* **2012**, *8*, 6198−6205.
(46) Waigh, T. A. Microrheology of Complex Fluids. *Rep. Prog. Phys.* **2005**, *68*, 685−742.
(47) Mason, T. G.; Ganesan, K.; van Zanten, J. H.; Wirtz, D.; Kuo, S. C. Particle Tracking Microrheology of Complex Fluids. *Phys. Rev. Lett.* **1997**, *79*, 3282−3285.
(48) Squires, T. M.; Mason, T. G. Fluid Mechanics of Microrheology. *Annu. Rev. Fluid Mech.* **2010**, *42*, 413−438.
(49) Mason, T. G. Estimating the Viscoelastic Moduli of Complex Fluids Using the Generalized Stokes-Einstein Equation. *Rheol. Acta* **2000**, *39*, 371−378.
(50) Mason, T. G.; Weitz, D. A. Optical Measurements of Frequency-Dependent Linear Viscoelastic Moduli of Complex Fluids. *Phys. Rev. Lett.* **1995**, *74*, 1250−1253.
(51) West, J. L.; Hubbell, J. A. Polymeric Biomaterials with Degradation Sites for Proteases Involved in Cell Migration. *Macromolecules* **1999**, *32*, 241−244.
(52) Patterson, J.; Hubbell, J. Enhanced Proteolytic Degradation of Molecularly Engineered PEG Hydrogels in Response to MMP-1 and MMP-2. *Biomaterials* **2010**, *31*, 7836−7845.
(53) Schultz, K. M.; Anseth, K. S. Monitoring Degradation of Matrix Metalloproteinases Cleavable PEG Hydrogels via Multiple Particle Tracking Microrheology. *Soft Matter* **2013**, *9*, 1570−1579.
(54) Fairbanks, B. D.; Schwartz, M. P.; Bowman, C. N.; Anseth, K. S. Photoinitiated Polymerization of PEG-Diacrylate with Lithium Phenyl-2,4,6-trimethylbenzoylphosphinate: Polymerization Rate and Cytocompatibility. *Biomaterials* **2009**, *30*, 6702−6707.
(55) Fairbanks, B. D.; Schwartz, M. P.; Halevi, A. E.; Nuttelman, C. R.; Bowman, C. N.; Anseth, K. S. A Versatile Synthetic Extracellular

https://doi.org/10.1021/acsbiomaterials.1c00871
ACS Biomater. Sci. Eng. XXXX, XXX, XXX−XXX

Matrix Mimic via Thiol-Norbornene Photopolymerization. *Adv. Mater.* **2009**, *21*, 5005−5010.
(56) Holzheimer, R. G.; Steinmetz, W.-G. Local and Systemic Concentrations of Pro- and Anti-Inflammatory Cytokines in Human Wounds. *Eur. J. Med. Res.* **2000**, *5*, 347−355.
(57) Crocker, J. C.; Grier, D. G. Methods of Digital Video Microscopy for Colloidal Studies. *J. Colloid Interface Sci.* **1996**, *179*, 298−310.
(58) Savin, T.; Doyle, P. S. Static and Dynamic Errors in Particle Tracking Microrheology. *Biophys. J.* **2005**, *88*, 623−638.
(59) Crocker, J. C.; Weeks, E. R. Particle Tracking Using IDL, 2011. http://www.physics.emory.edu/~weeks/idl/index.html (Dec, 2019).
(60) Schultz, K. M.; Baldwin, A. D.; Kiick, K. L.; Furst, E. M. Measuring the Modulus and Reverse Percolation Transition of a Degrading Hydrogel. *ACS Macro Lett.* **2012**, *1*, 706−708.
(61) Larsen, T.; Schultz, K.; Furst, E. M. Hydrogel Microrheology Near the Liquid-Solid Transition. *Korea-Aust. Rheol. J.* **2008**, *20*, 165−173.
(62) Wehrman, M. D.; Lindberg, S.; Schultz, K. M. Quantifying the Dynamic Transition of Hydrogenated Castor Oil Gels Measured via Multiple Particle Tracking Microrheology. *Soft Matter* **2016**, *12*, 6463−6472.
(63) Corrigan, A. M.; Donald, A. M. Passive Microrheology of Solvent-Induced Fibrillar Protein Networks. *Langmuir* **2009**, *25*, 8599−8605.
(64) Larsen, T. H.; Furst, E. M. Microrheology of the Liquid-Solid Transition During Gelation. *Phys. Rev. Lett.* **2008**, *100*, No. 146001.
(65) Escobar, F.; Anseth, K. S.; Schultz, K. M. Dynamic Changes in Material Properties and Degradation of Poly(ethylene glycol)-Hydrazone Gels as a Function of pH. *Macromolecules* **2017**, *50*, 7351−7360.
(66) Adolf, D.; Martin, J. E. Time-Cure Superposition During Crosslinking. *Macromolecules* **1990**, *23*, 3700−3704.
(67) Zhang, H.; Wehrman, M. D.; Schultz, K. M. Structural Changes in Polymeric Gel Scaffolds around the Overlap Concentration. *Front. Chem.* **2019**, *7*, No. 317.
(68) Diegelmann, R. F.; Evans, M. C.; et al. Wound healing: an overview of acute, fibrotic and delayed healing. *Front. Biosci.* **2004**, *9*, 283−289.
(69) Bakin, A. V.; Safina, A.; Rinehart, C.; Daroqui, C.; Darbary, H.; Helfman, D. M. A critical role of tropomyosins in TGF-β regulation of the actin cytoskeleton and cell motility in epithelial cells. *Mol. Biol. Cell* **2004**, *15*, 4682−4694.
(70) Edlund, S.; Landstrom, M.; Heldin, C.-H.; Aspenstrom, P. Transforming growth factor-β−induced mobilization of actin cytoskeleton requires signaling by small GTPases Cdc42 and RhoA. *Mol. Biol. Cell* **2002**, *13*, 902−914.

https://doi.org/10.1021/acsbiomaterials.1c00871
ACS Biomater. Sci. Eng. XXXX, XXX, XXX−XXX